

Cross-Shore Flow and Implications for Carbon Export in the California Current Ecosystem: A Lagrangian Analysis

Pierre Chabert, Francesco d'Ovidio, Vincent Echevin, Michael Stukel, Mark D. Ohman

▶ **To cite this version:**

Pierre Chabert, Francesco d'Ovidio, Vincent Echevin, Michael Stukel, Mark D. Ohman. Cross-Shore Flow and Implications for Carbon Export in the California Current Ecosystem: A Lagrangian Analysis. Journal of Geophysical Research. Oceans, 2021, 126 (2), pp.e2020JC016611. 10.1029/2020JC016611 . hal-03150447

HAL Id: hal-03150447
https://hal.science/hal-03150447

Submitted on 23 Aug 2022

HAL is a multi-disciplinary open access archive for the deposit and dissemination of scientific research documents, whether they are published or not. The documents may come from teaching and research institutions in France or abroad, or from public or private research centers.

L'archive ouverte pluridisciplinaire **HAL**, est destinée au dépôt et à la diffusion de documents scientifiques de niveau recherche, publiés ou non, émanant des établissements d'enseignement et de recherche français ou étrangers, des laboratoires publics ou privés.

Copyright

Check for updates

JGR Oceans

RESEARCH ARTICLE
10.1029/2020JC016611

Key Points:

- The extension of elevated chl-a waters covaries with the intensity of offshore transport diagnosed from satellite-derived currents
- Offshore sites of elevated carbon export are associated with advection of chlorophyll-rich coastal waters
- Climate forcing by ENSO and the NPGO accounts for much of the interannual variability in offshore extent of chlorophyll-rich coastal waters

Supporting Information:

- Supporting Information S1

Correspondence to:
P. Chabert,
pierre.chabert@locean-ipsl.upmc.fr

Citation:
Chabert, P., d'Ovidio, F., Echevin, V., Stukel, M. R., & Ohman, M. D. (2021). Cross-shore flow and implications for carbon export in the California current ecosystem: A Lagrangian analysis. *Journal of Geophysical Research: Oceans*, *126*, e2020JC016611. https://doi.org/10.1029/2020JC016611

Received 17 JUL 2020
Accepted 14 DEC 2020

© 2020. American Geophysical Union. All Rights Reserved.

Cross-Shore Flow and Implications for Carbon Export in the California Current Ecosystem: A Lagrangian Analysis

P. Chabert[1], F. d'Ovidio[1], V. Echevin[1], M. R. Stukel[2], and M. D. Ohman[3]

[1]Sorbonne Université, CNRS, IRD, MNHN, Laboratoire d'Océanographie et du Climat: Expérimentations et Approches Numériques (LOCEAN-IPSL), Paris, France, [2]Department of Earth, Ocean, and Atmospheric Sciences, Florida State University, Tallahassee, FL, USA, [3]Integrative Oceanography Division, Scripps Institution of Oceanography, La Jolla, CA, USA

Abstract Eastern Boundary Current Upwelling Systems are regions of elevated primary production and carbon export and thus play a central role in the global carbon cycle. In these regions, nutrient upwelling occurs in a narrow region close to the coast, but primary production and carbon export are typically observed across a broader region. The fact that productive waters reach the open ocean has important consequences for the biological carbon pump, because such transport connects nutrient sources close to the coast to the deep carbon sinks of the offshore ocean. However, many aspects of this offshore transport are still not known. Here we address seasonal and interannual variability of upwelling-related cross-shore flows in the California current ecosystem (CCE) by employing Lagrangian diagnostics of horizontal transport inferred from satellite data. We define an advective age as the time a water parcel flowed offshore of the 500 m isobath. We find that the offshore extension of high Chl-a waters covaries with the age of a coastal water parcel, and is consistent with mesoscale circulation. Interannual variability in the offshore extent of older waters is primarily driven by mesoscale variability and covaries with large scale forcing by both ENSO and the NPGO. The measured ratio of in-situ new production: carbon export also covaries with water age, and tends to be $\gg 1$ in younger and more balanced in older waters. Our results may help to parameterize the role of the finescale on the export of carbon in upwelling regions for climate resolving models.

Plain Language Summary The California current ecosystem (CCE) is a region of strong coastal upwelling, elevated organic matter production and high carbon flux into the deep ocean, and potentially influential in the global carbon cycle. Previous studies have suggested that production and sinking are not balanced in the CCE: there is more production than sinking close to the coast and more sinking than production offshore. Our study uses satellite measurements to analyze cross-shore flows in the CCE and assess whether horizontal transport of water, nutrients, and plankton can reconcile this spatial imbalance. By following water parcel trajectories, we find that the time since a water parcel is transported from the coast to the offshore is a predictor of whether the water parcel is a net source of organic matter (greater new production than sinking) or a net sink (greater sinking than new production). We find that the offshore distance of water transport varies strongly from year to year and is related to known sources of climate forcing, including El Nino-Southern Oscillation and the North Pacific Gyre Oscillation. Future organic matter exchanges between the coast and the offshore can be estimated thanks to covariability with these climate indices.

1. Introduction

In Eastern boundary upwelling systems (EBUS), winds blow alongshore during the upwelling season, causing nutrient-replete deep waters to come to the euphotic zone through divergence of Ekman transport at the coast, stimulating elevated net primary production (NPP) and inorganic carbon uptake. This primary production induces secondary production, the recycling of nutrients, and export of organic carbon into the aphotic zone. EBUSs are strongly advective systems: Ekman currents, as well as intense geostrophic mesoscale eddies and filaments, transport nearshore surface water offshore. The transport of organic matter (OM) from formation sites to export sites, occurs in three-dimensional space: the location of carbon export may be offset spatially from the region of elevated PP (Gruber et al., 2011; Olivieri & Chavez, 2000; Plattner et al., 2005). Accurately representing the processes and spatial locations of carbon production and export is

key for constraining the ocean carbon cycle in coupled model intercomparison project (CMIP) Earth System and other models (Richter, 2015; Small et al., 2015). At present, such cross-shore fluxes of OM are poorly represented in these models and it is not clear whether they show predictable seasonality or any relationship to large-scale climate forcing.

EBUS modeling is challenging because of the spatial and temporal variability that occurs at multiple scales (Marchesiello et al., 2003), their sensitivity to climate forcing, and the complexity of biophysical coupled processes (K. K. Liu et al., 2010). The North Pacific EBUS along the northwest American coast is known as the California current system (CCS). Many research efforts have been carried out to better understand CCS circulation and California current ecosystem (CCE) dynamics and responses to climate forcing (Goericke & Ohman, 2015). In the CCS, for much of the year—but primarily in spring and summer (Di Lorenzo, 2003)—winds blow equatorward along the California coast. Ekman currents transport coastal waters to the open ocean, inducing an upwelling of waters typically from depths of 100–200 m, although source waters change with the state of the Pacific decadal oscillation (PDO, [Chhak & Lorenzo, 2007]).

Previous studies in the CCE have shown that new production (i.e., production based on upwelled nitrate) tends to exceed carbon exported vertically below the euphotic zone in the nearshore region, where new and primary production is maximal (Chavez et al., 1991; Kranz et al., 2020; Plattner et al., 2005; Stukel et al., 2011). This imbalance is reduced and possibly compensated further offshore (Stephens et al., 2020; Stukel et al., 2011), with lower than expected vertical carbon export close to shore and higher than expected vertical carbon export further offshore. A hypothesis that would explain this spatial imbalance is that inorganic carbon is fixed in the nearshore region and then exported by the cross-shore circulation from nearshore sites of production to offshore sites of export. Such cross-shore transport could be caused by three main mechanisms: advection by surface Ekman currents, cold filaments of coastal origin, and westward propagating mesoscale eddies (Amos et al., 2019; Barth et al., 2005; Chenillat et al., 2016; Nagai et al., 2015). An example of this situation arises in the area off Point Conception (34.4°N) in Southern California. This is a site of elevated primary production (Kahru et al., 2009) but also the triggering location of strong meanders potentially evolving into mesoscale filaments and eddies in summer (Centurioni et al., 2008; Marchesiello et al., 2003).

Although the physical processes associated with cross-shore transport are well known, surprisingly little is known about its interannual variability. In addition, there are few long-term observational datasets of production and export (Kelly et al., 2018). This lack of knowledge has wider consequences, and in particular limits our capacity to predict biogeochemical responses of the CCE to future climate variability. Therefore, in this study, we address the following questions: (i) What is the length scale, and associated seasonal variability, of cross-shore transport in the CCE? (ii) What is the magnitude of interannual variability of cross-shore transport? (iii) Is this variability related to known sources of climate forcing, that would enable it to be represented in climate-resolving models? (iv) What consequences do variations in cross-shore transport have for organic carbon production and export? These questions are addressed through the analysis of highly energetic coastal upwelling meanders in the CCE, combining multi-satellite observations and in situ carbon export measurements with a Lagrangian analysis. We first describe the seasonality of the spatial patterns of the cross-shore transport and use them to explain the spatial imbalance of new production and vertical carbon export in the CCE. Last, we analyze the interannual variability of cross-shore transport, and assess its relationship to climate variability.

2. Data Set and Methods

2.1. Satellite-Derived Currents

Transport analysis is based primarily on sea surface currents provided by the Copernicus Marine Environment Monitoring Service (CMEMS), which consists of nearly 26 years of multi-satellite merged altimeter data and wind stress data, here from January 1, 1994 to October 20, 2019. The spatial resolution is $0.25° \times 0.25°$ (≈25 km at mid latitudes) and the temporal resolution is one day for the whole data set. The CMEMS (https://marine.copernicus.eu/) product used is the delayed time version until December 31, 2018 and the near real-time for January to October 2019. The surface currents consist of geostrophic velocities plus Ekman currents. Geostrophic velocities (U_G) are derived from the Absolute Dynamic Topography.

Ekman currents (U_E) are derived from wind data provided by the European Centre for Medium-Range Weather Forecasts (ECMWF) with a temporal resolution of 3 h and a spatial resolution of 1/4°. This product ($U = U_G + U_E$) is more appropriate than the purely geostrophic one, as Ekman currents are particularly important in upwelling systems. We compute total kinetic energy (TKE) maps from these currents with:

$$TKE = \frac{1}{2}(u^2 + v^2)$$

in which (u, v) are the components of the current for the x and y directions.

2.2. Lagrangian Water Age Model

We conducted a Lagrangian particle trajectory analysis of surface velocities. Our aim is to understand the spatial offset between nearshore production and export induced by horizontal transport. We thus follow the approach of d'Ovidio et al. (2015) and define an "offshore water age" as the time taken by the water parcel to be advected backward in time from its current position along its trajectory until it crosses the 500 m isobath. The rationale of this diagnostic is to detect filaments of coastal water advected offshore by horizontal transport and to estimate the time for water parcels in the filament to leave the coastal area. For example, a value of "20 days" assigned to a pixel means that the water parcel in that area was in the coastal area approximately 20 days before, where it was likely enriched in nutrients. A cutoff for the trajectory integration is put at 90 days. This means that a parcel is not considered of coastal origin if the backward trajectory does not cross the 500 m isobath in the previous 90 days. This threshold is chosen heuristically based on the reliability of past studies that have compared altimetry-derived Lagrangian diagnostics and chlorophyll patches (see review in Lehahn et al. [2018]), for two reasons. First, for a temporal horizon longer than a season, we assume that the water parcel has been mixed together with the environmental water longer enough to have lost a coastal signature. Second, we consider that accumulated advection errors on the trajectories are too large to provide any meaningful result even in a statistical sense on a temporal horizon larger than a few months. This "offshore water age" diagnostic has been validated at mesoscale precision with satellite-derived Chl-a patches (d'Ovidio et al., 2015; Sergi et al., 2020), surface drifters (d'Ovidio et al., 2015), and lithogenic isotopes (Sanial et al., 2015). These studies, however, were conducted in the Southern Ocean. In the Results section we evaluate this diagnostic for the CCE and specifically in the context of our objectives. Although it would be desirable to begin tracking waters very close to shore, i.e. closer to the sources of upwelling at the coastal boundary, the satellite product we use provides unreliable measures in close proximity to the continental boundary. Hence, we chose the 500 m isobath as the defining limit of inshore waters for this study. We assume that the time lapse between upwelling into the mixed layer and crossing of the 500 m isobath is of the order of a few days or less, thus negligible in respect to the time scales (10–90 days) considered here for offshore transport. We computed water age snapshots every 4 days (this time step was chosen to reduce the data set size without missing any dynamics) for 26 years (92 snapshots per year) of satellite data (between 1994 and 2019). This led to 2,374 snapshots, and a typical field of water age is shown for July 4, 2007 in Figure 1b. The white areas represent the water parcels that had not crossed the 500 m isobath in the last 90 days prior to July, 4. We computed the water age maps at a spatial resolution of 0.05° ≈ 5.5 km.

2.3. Satellite Chl-*a* Data

We compare Chl-a images (see example in Figure 1a) to the stirring patterns predicted by the Lagrangian analysis applied to the surface velocities. To achieve this, we use a multi-satellite product with daily sampling interval and 4 km of spatial resolution ([Kahru et al., 2015; Kahru et al., 2012] https://www.wimsoft.com/CC4km.htm). The temporal coverage of this data set is from 2002 to 2019. We processed data only during the lifetime of MODIS Aqua to avoid temporal interruptions. In order to compute anomalies of annual averages of ocean color images, we applied the following processing: we masked pixels under 1 $mg.m^{-3}$ in order to focus on high surface Chl-a concentrations. In the analysis presented in Section 3.1, similar processing was applied to the water age to select only water ages younger than 30 days. We consider 30 days to be the threshold below which the strongest correlation with Chl-a concentration appears.

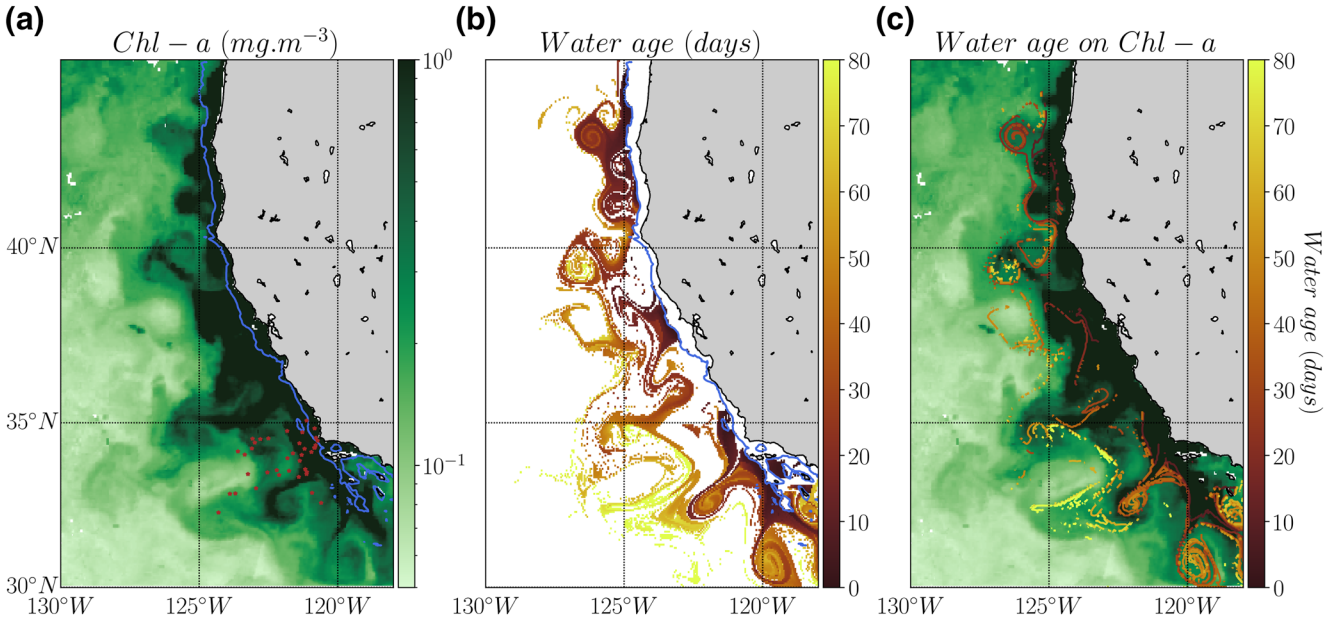


Figure 1. Snapshots of (a) the near-surface Chl-a concentration from MODIS Aqua (mg m^{-3}), (b) our Lagrangian diagnostic water age (days) and (c) the water age contours (levels are 10 days intervals from 0 to 80 days) superimposed on the near-surface Chl-a concentration (same colormap as panel a) over the CCE on July 4, 2007. Brown dots in (a) indicate the locations of the in-situ measurements. Light blue line in panels (a) and (b) indicates the 500 m isobath. CCE, California current ecosystem.

2.4. In situ Measurements

In situ measurements (Figure 1a, brown dots) were made during 2–5 days quasi-Lagrangian experiments on eight cruises of the CCE-LTER Program (CCE—Long Term Ecological Research, [Ohman et al., 2013; Stukel et al., 2015]). Dissolved nutrients (here $Si(OH)_4$, NO_3^-, PO_4) were analyzed by continuous flow segmented autoanalyzer (https://www.calcofi.org/about-calcofi/methods/422-nutrient-methods.html) based on Niskin bottle samples taken from surface waters. New production (computed from $^{15}NO_3^-$ uptake) and net primary productivity (hereafter NPP, computed from $H^{14}CO_3^-$ uptake) were measured in situ on a drifting incubation array (Kranz et al., 2020; Landry et al., 2009; R. M. Morrow et al., 2018). On cruises where $^{15}NO_3^-$ uptake data were not available, equations from K. K. Liu et al. (2010) were used to estimate the f-ratio from NO_3^-, NH_4^+, photosynthetically active radiation, and chlorophyll measurements. New production was then computed as primary productivity/6.625 × f-ratio. New production measurements based on $^{15}NO_3^-$ uptake can overestimate true nitrate uptake if substantial euphotic zone nitrification occurs, although this issue appears to be minor in the CCE (Stephens et al., 2020; Yool et al., 2007) Sinking carbon vertical fluxes were measured using $^{238}U - ^{234}Th$ disequilibrium and surface-tethered drifting sediment traps positioned at the base of the euphotic zone (Stukel & Barbeau, 2020; Stukel et al., 2019). Sinking particle flux was typically measured 20–40 m beneath the depth of the euphotic zone. It was normalized to the base of the euphotic zone using an exponential model of flux attenuation following Stukel et al. (2015). For further details, see supporting information.

2.5. Climate Indices

We compare the variability of cross-shore transport patterns with large scale physical forcing indexes. The North Pacific Gyre Oscillation (NPGO, Di Lorenzo et al. [2008], http://www.o3d.org/npgo/) is the second Empirical Orthogonal Function of Sea Surface Height variability in the Northeast Pacific. It represents the wind-driven, basin-scale decadal variability of the North Pacific Gyre circulation. Fluctuations in the NPGO are driven by regional and basin-scale variations in wind-driven upwelling and horizontal advection, controlling salinity and nutrient concentrations in the CCE. Detrended San Diego Sea Level Anomaly, averaged

for December-January-February (SDSLA_DJF) is an index of El Niño Southern Oscillation (ENSO) influence on the CCE (Lilly & Ohman, 2018). It is high during El Niño as elevated sea level in the equatorial band propagates along the coasts of central America, Mexico and California. High sea level is associated with a deeper than usual thermocline/nutricline and lower nearshore primary production.

2.6. Interannual Variability

In order to assess interannual variability of the water age distribution, we compute the average (between 30°N and 40°N) distance to shore of a specific water age (e.g., 60 days waters) for each snapshot. Concerning the area occupied by high Chl-a and young water age events, we compute the number of pixels concerned and multiply by the area of one pixel for each snapshot. We then compute annual means and anomalies relative to the global mean. Similar processing is applied for the TKE, SDSLA_DJF and NPGO. Area occupied by high Chl-a and young water age events, specific water age distance-to-shore and TKE spatial averages are made between 30° and 40°N in order to obtain smooth averages. Smaller spatial averaging windows were tested and found to provide less smooth results, but with similar correlation coefficients.

3. Results

3.1. Offshore Extension of Chl-a Patterns is Largely Driven by Horizontal Stirring

Figure 1 illustrates a qualitative comparison between spatial patterns of the Lagrangian water age diagnostic and Chl-a concentration. Regions of elevated phytoplankton (Chl-a > 1 mg.m^{-3}, Figure 1a) are generally associated with recently upwelled young waters (age < 30 days, Figure 1b). Mesoscale pathways are well captured by the age model. For example, at 127°W, 39°N, a high Chl-a location co-occurs with an elongated filament transporting relatively young water. Another chlorophyll-rich young coastal filament is also detectable between the coast (123°W, 37°N) and offshore (124°W, 34°N) (Figures 1a and 1b). Young water parcels are observed near the coast but also offshore, where they are rapidly advected by filaments and eddies. Older water ages are typically found offshore, sometimes around eddies as offshore older water is entrained. Patches of older waters can also be found in nearshore areas, where recirculation can trap water parcels for long (several tens of days) periods. Note also the nearshore regions without water age values (e.g. 35–37°N, Figure 1b), likely due to imperfect coastal current data which prevents the advection of particles from and to this coastal sector.

In general, elevated Chl-a concentrations can be found both nearshore and offshore but a visual comparison with patterns of water age suggests that they are more associated with younger water patches than old ones. In order to quantify this relation, we estimate the area occupied by patterns of high Chl-a and young water on a daily basis between 2002 and 2018 and compare the temporal variability of their offshore extension. This test is more robust than a filament-by-filament (pixel-by-pixel) comparison, which is notoriously resistant to quantitative validation because altimetry errors may easily displace a filament a distance of the same order as the filament width.

The results of the comparison between the areas occupied by high Chl-a patterns and filaments of young waters is depicted in Figure 2. On a seasonal time scale, these two areas are strongly correlated (Figure 2a, $r = 0.93$, $p < 0.001$). A maximal extension of chlorophyll-rich waters is reached in June, which coincides with the strongest alongshore wind stress, Ekman transport and associated coastal upwelling of nitrate-enriched water (e.g. Jacox et al. [2018]). On an interannual time scale (between 2002 and 2018), the two indices also covary significantly (Figure 2b, $r = 0.63$, $p < 0.01$). Interestingly both indices reach their lowest values in 2014 (water age) and 2015 (Chl-a) during the North Pacific warm anomaly (Di Lorenzo & Mantua, 2016).

3.2. Carbon Export Balances New Production in Regions where Offshore Water Age is Greater than 60 Days

As a second step, we test for a relationship between the offshore water age and the ratio between new production and sinking carbon export (NP and CE), after normalization of NP to carbon units assuming

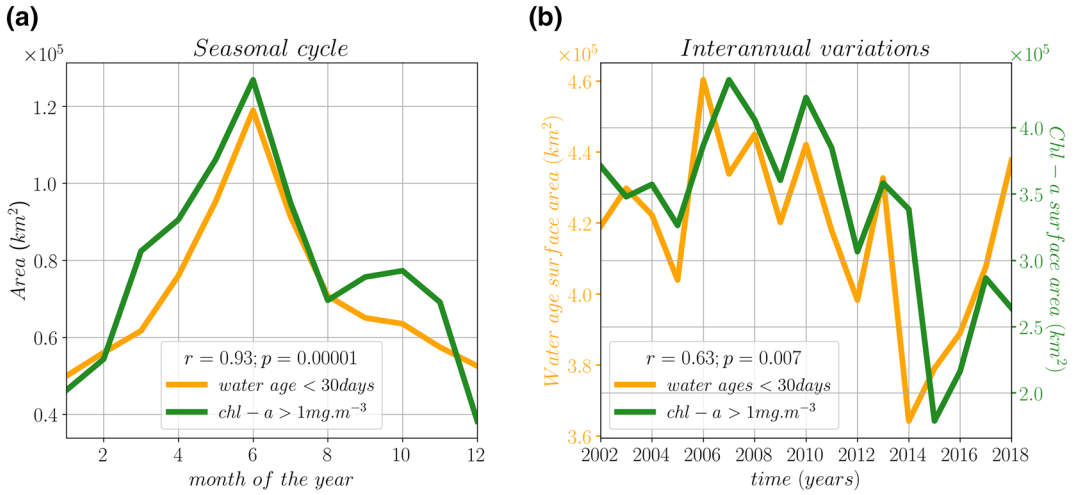


Figure 2. Area occupied by high Chl-a events (>1 mg m^{-3}, green line, right axis) and area occupied by young water age events (<30 days, orange line, left axis). (a) Mean seasonal cycle ($r = 0.93$; $p < 0.01$ between the two signals) and (b) interannual variability ($r = 0.63$; $p < 0.01$ between the two signals). Averaged between 30° and 40°N.

Redfield C:N stoichiometry. Our working hypothesis is that horizontal stirring translates the temporal lag between NP and CE into a spatial offset, and that the offshore water age diagnostic can capture this spatio-temporal relation. Thanks to extensive process studies (Goericke & Ohman, 2015), in situ measurements of surface nutrients (silicic acid, nitrate and phosphate), NPP, CE and NP:CE are available in the CCE region, in particular between 32°N and 35°N (locations are marked by brown dots in Figure 1a). We thus compare in-situ measurements with satellite-derived water ages for the same day and location using negative exponential regressions. Other functions (linear and power law) were tested but show no significance or lower *r*-values (not shown). We find that surface nutrients (silicic acid, nitrate and phosphate, Figures 3a–3c) concentrations decay exponentially with water age. These relationships validate our hypothesis that Lagrangian trajectories are initiated in a nutrient rich environment. Accordingly, we find that NPP varies inversely with water age (Figure 3d), as expected in a system in which recent upwelling is a source of new nutrients to stimulate production. The relatively high correlation value between surface nutrients and water age is similar to the correlation value between NPP and water age ($-0.73 < r < -0.68$). As water parcels age, surface nutrients are drawn down and NPP decreases. Similarly, we found that carbon export was higher in younger age waters, although carbon export declines less rapidly with water age (Figure 3e). To assess how the balance between NP and CE changes with water parcel age, we also compared water age to the ratio of NP:CE in these water parcels (Figure 3f). We again found a statistically significant relationship, showing that younger water parcels had new production rates that substantially exceeded contemporaneous sinking particle flux. However, after 60 days, new production and export reach an equilibrium. Water parcels older than this showed approximately balanced new production and export, on average. There was, however, still substantial variability in the NP:export ratios in these older water parcels, likely because as the water age increases, processes like vertical shear, mixing and subduction complicate the interpretation of a water parcel as having a single source and age.

A steady-state one-dimensional balance between NP and CE would lead to an expected ratio of these two properties of 1 for waters of all ages, meaning that all the NP generated in the euphotic layer would be exported vertically in the water column below. In contrast, we find that NP:CE is generally higher than 1 in younger waters and declines with water age (Figure 3f, $r = -0.46$). This suggests that a significant part of the organic carbon produced in the euphotic layer is not exported below the euphotic zone locally, but is advected horizontally along the water mass trajectory. Many ratios are found below the 1:1 line between water ages of 60–80 days, which implies that in such waters the sinking organic carbon originating from other locations has been advected to the measurement sites. This situation occurs for a wide range of distances to shore (between 100 km and 400 km; Figure 3f). Except for surface nutrients and NPP (which are less correlated with distance-to-shore than the water age), distance-to-shore is not linearly correlated ($p > 0.1$) with

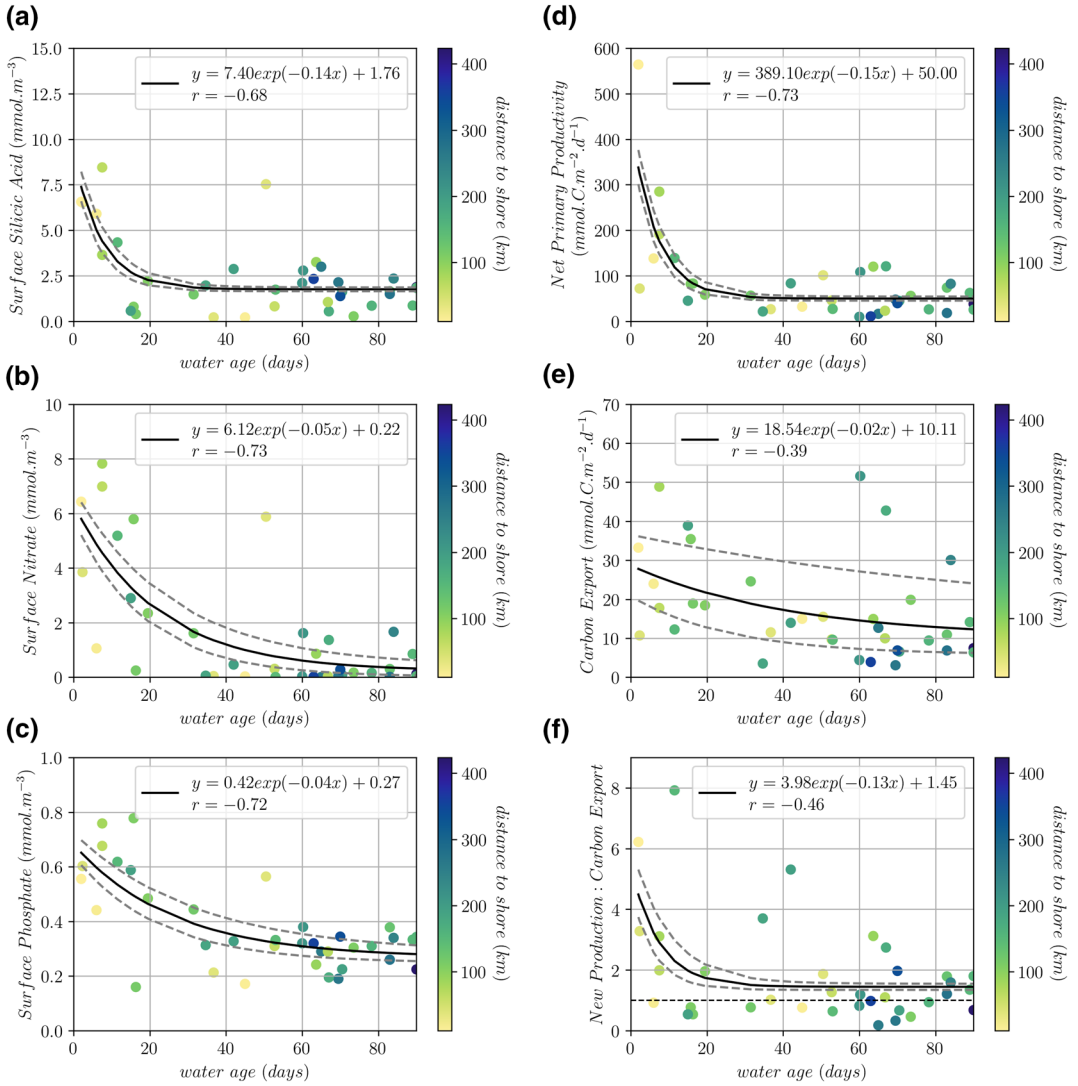


Figure 3. Relationship between water age and measured in situ: (a) surface slicic acid (mmol m^{-3}), (b) surface nitrate (mmol m^{-3}), (c) surface phosphate (mmol m^{-3}) (d) net primary production (mmol C m^{-2}. d^{-1}), (e) vertical carbon export (mmol C m^{-2} d^{-1}), and (f) new production: Carbon Export ratio. Solid black lines indicate negative exponential regressions, gray dashed lines indicate 95% confidence intervals (C.I.) and horizontal dashed line in (f) indicates the equilibrium New Production: Carbon Export ratio of 1. Colors of symbols indicate the distance to shore.

variables shown in Figure 3 (distance-to-shore and: surface nitrate: $r = -0.4$, $p = 0.01$; surface silicic acid: $r = -0.3$, $p = 0.07$; surface phosphate: $r = -0.34$, $p = 0.04$; NPP: $r = -0.4$, $p = 0.02$; CE: $r = -0.25$, $p = 0.14$; NP:CE, $r = -0.2$, $p = 0.24$). Only surface Silicic Acid shows a significant negative exponential relationship with distance-to-shore, however less correlated ($r = -0.44$) than with the water age. This result shows that our simple water age index, which takes into account the history of the water mass since it has left the nutrient-rich coastal area, is strongly preferred over proximity to the coast as a predictor of biogeochemical characteristics related to organic carbon production and vertical export.

3.3. Seasonal Variability of Cross-Shore Flow and Inferred C Export

We analyze the seasonal and spatial variability of the probability of occurrence of waters of different ages, for the primary upwelling season (May–September, Figure 4). We display probabilities for occurrence of water ages of: (a) 0–20 days and (b) 60–80 days. Young ages (0–20 days, Figure 4a—upper row) are more likely

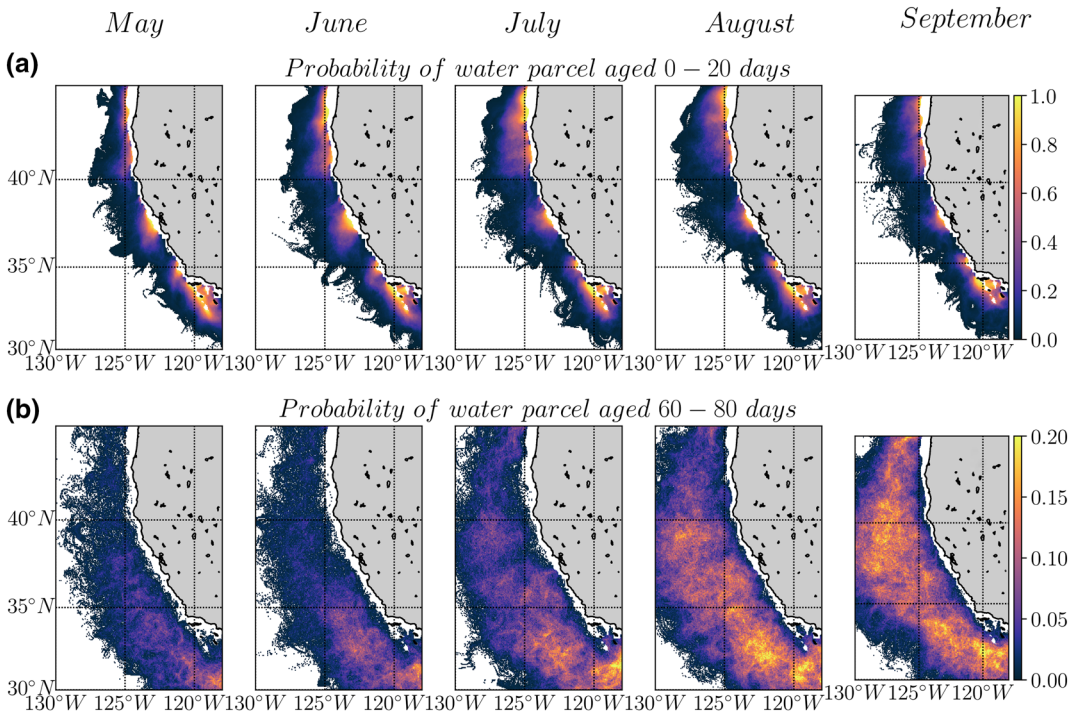


Figure 4. Climatological maps indicate the probability of occurrence of an: (a) 0–20 days and (b) 60–80 days water age event during the upwelling season (from May to September).

to occur near the coast between 32°−35°N, 37°−38°N, and north of 40°N. In the former regions, the month-to-month variability is weak while in the latter (northern) region, the seasonal cycle is more pronounced and reaches its peak in July. These locations with highest probability are limited in space, concentrated nearshore and coincide with the most intense upwelling cells along the California coast. There are locations along the coast (around 36°N) with low probability of occurrence, likely due to imperfect coastal current data (see the Discussion for details). High probabilities for occurrence of young water ages correspond to regions of elevated primary production (Figure 3). In other words, Figure 4 (upper row) also corresponds to the locations where NP is most likely to dominate.

At the beginning of the upwelling season, the probability of occurrence of old ages is higher south of 40°N than in the northern region where the upwelling season tends to start later and be shorter (Bograd et al., 2009). As the upwelling season progresses, areas of high probability of occurrence of old waters appear, corresponding to young waters upwelled earlier in the season that have been evolving. Old waters are more likely to occur in a broad region from the shore to up to 800 km offshore, in which upwelled waters have been advected and stirred. Based on the results in Figure 3, high probability for occurrence of old water ages correspond to regions where vertical carbon export tends to be close to or slightly exceed NP, i.e. where CE is most likely to dominate. To test the robustness of the seasonal patterns, we computed averages over several distinct time intervals (years [1993; 2003], [2003; 2013] and [2013; 2019]) and found similar spatial patterns (not shown). Also, removing ENSO events based on a San Diego Sea Level Anomaly criterion (>50 mm anomaly for >1 month) does not significantly affect the pattern and the seasonal cycle (not shown). Thus, we find that the climatological patterns of inferred carbon export hotspots shown in Figure 4 are reliable.

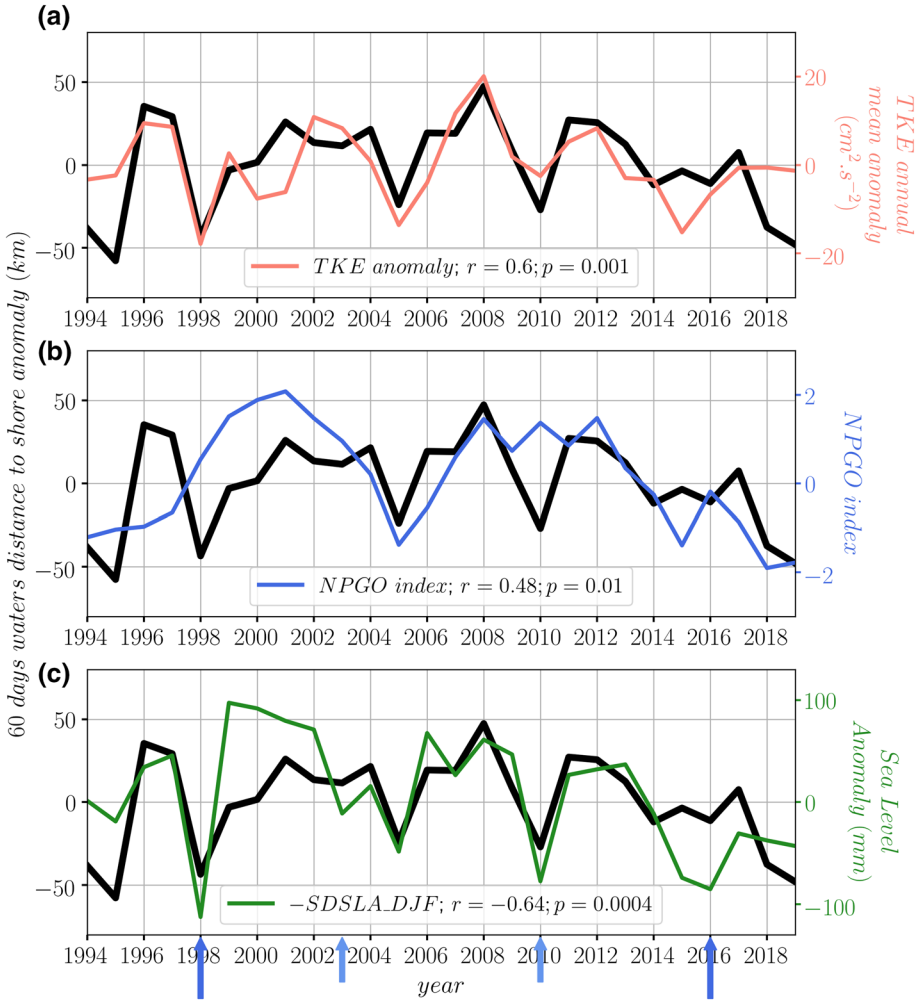


Figure 5. Interannual variability of annual averages of anomalies of distances-to-shore of 60 day old water (black line) against (a) Eddy Kinetic Energy (EKE, salmon line), (b) NPGO index (blue line) and (c) San Diego Sea Level Anomaly in December, January and February (-SDSLA_DJF, scale reversed, green line). Light blue arrows indicate California El Niño years and darker blue long arrows indicate the strongest El Niños years. NPGO, North Pacific gyre oscillation.

3.4. Interannual Variability of Offshore Extent of Flow

The 26 years satellite record enables us to compare interannual variability in water age, as a proxy for production and export, with important climate drivers. For this purpose, we consider 60 days water as a critical water age that tends to indicate balanced NP: CE (cf. Figure 3f).

We find that the annual average anomalies of the distance-to-shore of the critical water age (60 days) covaries with TKE (Figure 5a, $r = 0.66$, $p < 0.01$), the NPGO (Figure 5b, $r = 0.48$, $p = 0.01$), and with San Diego Sea Level Anomaly, as an index of ENSO in the CCE (Figure 5c, $r = -0.64$, $p < 0.001$). Moderate-to-strong El Niño events (like 1998, 2010, and 2016, blue arrows on Figure 5) tend to be associated with negative TKE anomalies and therefore with reduction in mesoscale activity, with concomitant reduction of the offshore extent of the region where NP and CE are most likely to be balanced. Conversely, this region presents greater offshore extent as La Niña events tend to be associated with positive TKE, and therefore stronger mesoscale activity.

4. Discussion

Advective processes, working at multiple spatial and temporal scales, reshape biogeochemical patterns in the pelagic ocean (Frischknecht et al., 2018; Resplandy et al., 2012). Horizontal transport leads to decoupling of net community production, new production, and export production at the mesoscale, obfuscating relationships between these and other processes (Estapa et al., 2015; Kranz et al., 2020). At the same time, mesoscale eddies, fronts, and filaments can act as sites of enhanced vertical transport leading to upwelling or downwelling with concomitant passive export of advected organic matter (Levy et al., 2013; Omand et al., 2015; Resplandy et al., 2019; Stukel et al., 2017). Understanding—and predicting—the impacts of horizontal transport on processes relevant to the biological pump is crucial to constraining different pathways of carbon transport to the ocean interior (e.g., sinking particles, diel vertical migration, active transport; [Boyd et al., 2019; Ducklow et al., 2001]). The existence of a spatial discrepancy between regions when nutrients are injected and regions where organic matter sinks is especially relevant in upwelling systems (Plattner et al., 2005). Without offshore advection of high biomass water parcels, most carbon export would remain confined at the upwelling sites. Intense offshore advection events, however, have the potential to drive export pulses in the deep ocean with important consequences for open ocean mesopelagic and benthic communities (Smith et al., 2018). The stirring process at the origin of the offshore transport however involves the interaction of fine scale features and creates patterns with a complex geometry. Understanding the variability of this offshore transport, and linking it to the large-scale dynamics—in particular to modes of climate variability—is especially relevant for climate-resolving models, which cannot explicitly resolve the subgrid details of the stirring process (Bourgeois et al., 2016), and therefore cannot properly represent where the organic matter produced in the upwelled region eventually sinks.

Explicit coupling of finescale Lagrangian water parcel transport estimates with in situ biological pump measurements is a powerful approach to elucidating how NP, NPP, and CE are related in time and space. In this study, satellite-derived Lagrangian water age diagnostics made it possible to infer the duration and lateral extent of cross-shore flows in the CCE. We found that independent measurements of NP and sinking CE are directly related to these water age diagnostics. In younger waters (i.e., those that more recently occurred closer to shore), there is an excess of NP over CE, but in older waters (60–80 days since emerging from the coast), there is a closer balance between NP and CE. Our 26-years record of water age diagnostics revealed that both seasonal and interannual scale variations in these inferred cross-shore flows are related to the areal extent of elevated Chl-a, with a broader region of high phytoplankton concentrations occurring in seasons and in years of stronger offshore transport. These seasonal and longer term variations in phytoplankton concentrations, primary production, and carbon export are modulated by variations in mesoscale TKE, and by climate forcing represented by ENSO and the NPGO.

We show that the relationship between water age and different biogeochemical properties is a result of the covariability of nutrient concentrations with water age, i.e., the time since nutrients entered the euphotic zone near the coast via coastal upwelling. As water age increases, NP decreases as macronutrients are consumed and other trophic levels (zooplankton) begin to develop. With continuing depletion of macronutrients like nitrate and silicic acid, and temporal changes in the food web (Messié & Chavez, 2017), recycled nutrients play a greater role. However, new nutrients may also enter the surface water parcels via mixing and submesoscale addies in the offshore oligotrophic region (Kessouri et al., 2020).

Recent studies (Amos et al., 2019; Lovecchio et al., 2017) estimate organic carbon offshore transport in EBUS through lateral advection. Amos et al. (2019) describe eddy-induced offshore organic carbon enrichment, especially by cyclonic eddies, illustrating the major role played by eddies in the CCE regional carbon budget. This process is included in the present analysis because the Lagrangian water age diagnostic includes contributions by eddies, filaments, and Ekman transport. If used in association with other Lagrangian diagnostics (e.g., retention time, [d'Ovidio et al., 2015]) and with satellite-derived particulate organic carbon estimates (Amos et al., 2019), our water age diagnostics could be used to differentiate eddies and filaments and thus assess their respective roles in organic carbon offshore transport.

In order to qualitatively separate the influence of Ekman transport from geostrophic motions, we computed our same diagnostics including only the geostrophic component (purely geostrophic [PG], without considering winds; data not illustrated). We found no significant correlation between the seasonal cycle of the area

occupied by young water ages from the PG product and the area occupied by high Chl-a events, suggesting that ageostrophic motions must also be considered.

It is important to note that the cross-shore transport induced by these mesoscale eddies and filaments is not oriented solely offshore. The occurrence of old water parcels over a broad area (Figure 4) highlights not only the role of mixing in carbon export, but also the role of recirculation and retention that can in some cases lead export to occur near regions of elevated NP. This result underscores the importance of considering water age, rather than the classical distance-to-shore, as a proxy for carbon export.

This description emphasizes upwelling near the coastal boundary, without explicitly considering wind stress curl-induced upwelling (Capet et al., 2004; Chelton, 1982; Renault et al., 2016). Ekman pumping associated with positive wind stress curl can supply new nutrients to the euphotic zone offshore of the coastal boundary, with major consequences for primary production and higher trophic levels (Rykaczewski & Checkley, 2008) and potentially for carbon export. However, the region inshore of the 500 m isobath in the present study includes part of the domain of wind stress curl upwelling (Pickett & Paduan, 2003; Rykaczewski & Checkley, 2008), so this process is partially included in our analysis. Another limitation of our analysis is that in addition to macronutrients like nitrate, iron is also known to be a regionally important limiting micro-nutrient in some parts of the CCS (Brzezinski et al., 2015; Hutchins & Bruland, 1998; King & Barbeau, 2011; Messié & Chavez, 2015), and regions of severe Fe limitation may be spatially offset from regions of N limitation (King & Barbeau, 2007; Stukel et al., 2017). Furthermore, meso and submesoscale vertical dynamics which may enrich (e.g. [Kessouri et al., 2020]) or deplete (e.g., through subduction, [Gruber et al., 2011; Stukel et al., 2017]) the surface layer in the coastal transition zone are not resolved here. Last a limitation of current satellite altimetry is that horizontal mesoscale structures are much smoother (and currents weaker) than in reality because of time and space interpolation of along-track sea level observations. Submesoscale structures are not resolved by the satellite product, thus ageostrophic components and mixed-layer instabilities are not taken into account. Positional errors between Chl-a patterns and Lagrangian derived diagnostics (up to 20 km) can appear nearshore, and altimetry potentially underestimates geostrophic currents (Lehahn et al., 2018). Such errors could be estimated by a rigorous comparison of the positions of the Lagrangian structures derived from numerical trajectories with the ones obtained by analyzing real surface drifters (e.g., [Nencioli et al., 2011]). This type of error is expected to be largely reduced in the incoming years by next satellite missions like SWOT (R. Morrow et al., 2019).

5. Conclusion and Perspectives

By using satellite-derived Lagrangian water age diagnostics together with in situ measurements of surface nutrients concentrations, organic carbon production and vertical carbon export, we show that the most productive water parcels and those that are likely to vertically export the most carbon relative to local production can be differentiated. New production exceeds sinking particle export in younger waters, inferred to be recently upwelled. New production is more closely balanced by vertical export in older waters. A 26-years record of water age diagnostics identifies regions of inferred carbon export hotspots, whose spatial extent is associated with mesoscale ocean variability and modulated by large-scale sources of climate forcing that include ENSO and the NPGO. Therefore, it is possible to model at least a major part of this biogeochemically relevant cross-shore transport through its covariability with climate forcing. At the same time, the finding that some of the variability in carbon export is not related to larger scale physical forcing underscores the need for mesoscale and sub-mesoscale studies in order to fully represent carbon export in Earth System models. The Lagrangian water age diagnostic can also be used as a near real-time tool for decision making during filament-following oceanographic cruises, as it can provide locations where new production and carbon export are likely to be spatially decoupled.

Data Availability Statement

Water age maps, primary production and carbon export data are available in CCE-LTER's DataZoo (https://oceaninformatics.ucsd.edu/datazoo/catalogs/ccelter/datasets). Satellite data can be found at: Chla—https://www.wimsoft.com/CC4km.htm, surface currents—https://marine.copernicus.eu/; product identifier:

MULTIOBS_GLO_PHY_REP_015_004). The Lagrangian code we used is now part of the SPASSO package which can be downloaded here: https://spasso.mio.osupytheas.fr/.

Acknowledgments
This work has been partly supported by OCE-16-37632 from the U.S. National Science Foundation to the California Current Ecosystem LTER site, Cnes through the TOSCA project BIOSWOT-AdAC, the Gordon and Betty Moore Foundation to MDO, and benefited from the French state aid managed by the ANR under the "Investissements d'avenir" programme with the reference ANR-11-IDEX-0004 - 17-EURE-0006.

References

Amos, C. M., Castelao, R. M., & Medeiros, P. M. (2019). Offshore transport of particulate organic carbon in the California Current System by mesoscale eddies. *Nature Communications*, *10*(1), 4940. https://doi.org/10.1038/s41467-019-12783-5

Barth, J. A., Pierce, S. D., & Cowles, T. J. (2005). Mesoscale structure and its seasonal evolution in the northern California current system. *Deep Sea Research Part II: Topical Studies in Oceanography*, *52*(1), 5–28. https://doi.org/10.1016/j.dsr2.2004.09.026

Bograd, S. J., Schroeder, I., Sarkar, N., Qiu, X., Sydeman, W. J., & Schwing, F. B. (2009). Phenology of coastal upwelling in the California Current. *Geophysical Research Letters*, *36*, L01602. https://doi.org/10.1029/2008GL035933

Bourgeois, T., Orr, J. C., Resplandy, L., Terhaar, J., Ethé, C., Gehlen, M., & Bopp, L. (2016). Coastal-ocean uptake of anthropogenic carbon. *Biogeosciences*, *13*(14), 4167–4185. https://doi.org/10.5194/bg-13-4167-2016

Boyd, P. W., Claustre, H., Levy, M., Siegel, D. A., & Weber, T. (2019). Multi-faceted particle pumps drive carbon sequestration in the ocean. *Nature*, *568*(7752), 327–335. https://doi.org/10.1038/s41586-019-1098-2

Brzezinski, M. A., Krause, J. W., Bundy, R. M., Barbeau, K. A., Franks, P., Goericke, R., et al. (2015). Enhanced silica ballasting from iron stress sustains carbon export in a frontal zone within the California Current. *Journal of Geophysical Research: Oceans*, *120*(7), 4654–4669. https://doi.org/10.1002/2015JC010829

Capet, X. J., Marchesiello, P., & McWilliams, J. C. (2004). Upwelling response to coastal wind profiles. *Geophysical Research Letters*, *31*, L13311. https://doi.org/10.1029/2004GL020123

Centurioni, L. R., Ohlmann, J. C., & Niiler, P. P. (2008). Permanent Meanders in the California Current System. *Journal of Physical Oceanography*, *38*(8), 1690–1710. https://doi.org/10.1175/2008JPO3746.1

Chavez, F. P., Barber, R. T., Kosro, P. M., Huyer, A., Ramp, S. R., Stanton, T. P., & Mendiola, B. R. d. (1991). Horizontal transport and the distribution of nutrients in the Coastal Transition Zone off northern California: Effects on primary production, phytoplankton biomass and species composition. *Journal of Geophysical Research*, *96*(C8), 14833–14848. https://doi.org/10.1029/91JC01163

Chelton, D. B. (1982). Large-scale response of the California Current to forcing by the wind stress curl. *California Cooperative Oceanic Fisheries Investigations Reports*, *XXIII*, 19.

Chenillat, F., Franks, P. J. S., & Combes, V. (2016). Biogeochemical properties of eddies in the California Current System. *Geophysical Research Letters*, *43*(11), 5812–5820. https://doi.org/10.1002/2016GL068945

Chhak, K., & Lorenzo, E. D. (2007). Decadal variations in the California Current upwelling cells. *Geophysical Research Letters*, *34*, L14604. https://doi.org/10.1029/2007GL030203

Di Lorenzo, E. (2003). Seasonal dynamics of the surface circulation in the Southern California Current System. *Deep Sea Research Part II: Topical Studies in Oceanography*, *50*(14–16), 2371–2388. https://doi.org/10.1016/S0967-0645(03)00125-5

Di Lorenzo, E., & Mantua, N. (2016). Multi-year persistence of the 2014/15 North Pacific marine heatwave. *Nature Climate Change*, *6*(11), 1042–1047. https://doi.org/10.1038/nclimate3082

Di Lorenzo, E., Schneider, N., Cobb, K. M., Franks, P. J. S., Chhak, K., Miller, A. J., et al. (2008). North Pacific Gyre Oscillation links ocean climate and ecosystem change. *Geophysical Research Letters*, *35*, L08607. https://doi.org/10.1029/2007GL032838

Ducklow, H., Steinberg, D., & Buesseler, K. (2001). Upper ocean carbon export and the biological pump. *Oceanography*, *14*(4), 50–58. https://doi.org/10.5670/oceanog.2001.06

d'Ovidio, F., Della Penna, A., Trull, T. W., Nencioli, F., Pujol, M.-I., Rio, M.-H., et al. (2015). The biogeochemical structuring role of horizontal stirring: Lagrangian perspectives on iron delivery downstream of the Kerguelen Plateau. *Biogeosciences*, *12*(19), 5567–5581. https://doi.org/10.5194/bg-12-5567-2015

Estapa, M. L., Siegel, D. A., Buesseler, K. O., Stanley, R. H. R., Lomas, M. W., & Nelson, N. B. (2015). Decoupling of net community and export production on submesoscales in the Sargasso Sea. *Global Biogeochemical Cycles*, *29*(8), 1266–1282. https://doi.org/10.1002/2014GB004913

Frischknecht, M., Münnich, M., & Gruber, N. (2018). Origin, transformation, and fate: The three-dimensional biological pump in the California Current System. *Journal of Geophysical Research: Oceans*, *123*(11), 7939–7962. https://doi.org/10.1029/2018JC013934

Goericke, R., & Ohman, M. D. (2015). Introduction to CCE-LTER: Responses of the California Current Ecosystem to climate forcing. *Deep Sea Research Part II: Topical Studies in Oceanography*, *112*, 1–5. https://doi.org/10.1016/j.dsr2.2014.12.001

Gruber, N., Lachkar, Z., Frenzel, H., Marchesiello, P., Münnich, M., McWilliams, J. C., et al. (2011). Eddy-induced reduction of biological production in eastern boundary upwelling systems. *Nature Geoscience*, *4*(11), 787–792. https://doi.org/10.1038/ngeo1273

Hutchins, D. A., & Bruland, K. W. (1998). Iron-limited diatom growth and Si:N uptake ratios in a coastal upwelling regime. *Nature*, *393*(6685), 561–564. https://doi.org/10.1038/31203

Jacox, M. G., Edwards, C. A., Hazen, E. L., & Bograd, S. J. (2018). Coastal upwelling revisited: Ekman, Bakun, and Improved Upwelling Indices for the U.S. West Coast. *Journal of Geophysical Research: Oceans*, *123*(10), 7332–7350. https://doi.org/10.1029/2018JC014187

Kahru, M., Kudela, R. M., Anderson, C. R., & Mitchell, B. G. (2015). Optimized merger of Ocean chlorophyll algorithms of MODIS-Aqua and VIIRS. *IEEE Geoscience and Remote Sensing Letters*, *12*(11), 2282–2285. https://doi.org/10.1109/LGRS.2015.2470250

Kahru, M., Kudela, R. M., Manzano-Sarabia, M., & Greg Mitchell, B. (2012). Trends in the surface chlorophyll of the California Current: Merging data from multiple ocean color satellites. *Deep Sea Research Part II: Topical Studies in Oceanography*, *77–80*, 89–98. https://doi.org/10.1016/j.dsr2.2012.04.007

Kahru, M., Kudela, R., Manzano-Sarabia, M., & Mitchell, B. G. (2009). Trends in primary production in the California Current detected with satellite data. *Journal of Geophysical Research*, *114*(C2). https://doi.org/10.1029/2008JC004979

Kelly, T. B., Goericke, R., Kahru, M., Song, H., & Stukel, M. R. (2018). CCE II: Spatial and interannual variability in export efficiency and the biological pump in an eastern boundary current upwelling system with substantial lateral advection. *Deep Sea Research Part I: Oceanographic Research Papers*, *140*, 14–25. https://doi.org/10.1016/j.dsr.2018.08.007

Kessouri, F., Bianchi, D., Renault, L., McWilliams, J. C., Frenzel, H., & Deutsch, C. A. (2020). Submesoscale currents modulate the seasonal cycle of nutrients and productivity in the California current system. *Global Biogeochemical Cycles*, *34*(10), e2020GB006578. https://doi.org/10.1029/2020GB006578

King, A. L., & Barbeau, K. (2007). Evidence for phytoplankton iron limitation in the southern California Current System. *Marine Ecology Progress Series*, *342*, 91–103. https://doi.org/10.3354/meps342091

King, A. L., & Barbeau, K. A. (2011). Dissolved iron and macronutrient distributions in the southern California Current System. *Journal of Geophysical Research*, *116*, C03018. https://doi.org/10.1029/2010JC006324

Kranz, S. A., Wang, S., Kelly, T. B., Stukel, M. R., Goericke, R., Landry, M. R., & Cassar, N. (2020). Lagrangian studies of marine production: A multimethod assessment of productivity relationships in the California Current ecosystem upwelling region. *Journal of Geophysical Research: Oceans*, *125*(6), e2019JC015984. https://doi.org/10.1029/2019JC015984

Landry, M. R., Ohman, M. D., Goericke, R., Stukel, M. R., & Tsyrklevich, K. (2009). Lagrangian studies of phytoplankton growth and grazing relationships in a coastal upwelling ecosystem off Southern California. *Progress in Oceanography*, *83*(1–4), 208–216. https://doi.org/10.1016/j.pocean.2009.07.026

Lehahn, Y., d'Ovidio, F., & Koren, I. (2018). A satellite-based Lagrangian view on phytoplankton dynamics. *Annual Review of Marine Science*, *10*(1), 99–119. https://doi.org/10.1146/annurev-marine-121916-063204

Levy, M., Bopp, L., Karleskind, P., Resplandy, L., Ethe, C., & Pinsard, F. (2013). Physical pathways for carbon transfers between the surface mixed layer and the ocean interior. *Global Biogeochemical Cycles*, *27*(4), 1001–1012. https://doi.org/10.1002/gbc.20092

Lilly, L. E., & Ohman, M. D. (2018). CCE IV: El Niño-related zooplankton variability in the southern California Current System. *Deep Sea Research Part I: Oceanographic Research Papers*, *140*, 36–51. https://doi.org/10.1016/j.dsr.2018.07.015

Liu, K.-K., Atkinson, L., Quiñones, R., & Talaue-McManus, L. (2010). *Carbon and nutrient fluxes in continental margins: A global synthesis*. Springer Science & Business Media.

Lovecchio, E., Gruber, N., Münnich, M., & Lachkar, Z. (2017). On the long-range offshore transport of organic carbon from the Canary Upwelling System to the open North Atlantic. *Biogeosciences*, *14*(13), 3337–3369. https://doi.org/10.3929/ethz-b-000190480

Marchesiello, P., Mcwilliams, J. C., & Shchepetkin, A. (2003). Equilibrium structure and dynamics of the California current system. *Journal of Physical Oceanography*, *33*, 31.

Messié, M., & Chavez, F. P. (2015). Seasonal regulation of primary production in eastern boundary upwelling systems. *Progress in Oceanography*, *134*, 1–18. https://doi.org/10.1016/j.pocean.2014.10.011

Messié, M., & Chavez, F. P. (2017). Nutrient supply, surface currents, and plankton dynamics predict zooplankton hotspots in coastal upwelling systems. *Geophysical Research Letters*, *44*(17), 8979–8986. https://doi.org/10.1002/2017GL074322

Morrow, R., Fu, L.-L., Ardhuin, F., Benkiran, M., Chapron, B., Cosme, E., et al. (2019). Global observations of fine-scale ocean surface topography with the Surface Water and Ocean Topography (SWOT) Mission. *Frontiers in Marine Science*, *6*, 232. https://doi.org/10.3389/fmars.2019.00232

Morrow, R. M., Ohman, M. D., Goericke, R., Kelly, T. B., Stephens, B. M., & Stukel, M. R. (2018). CCE V: Primary production, mesozooplankton grazing, and the biological pump in the California Current Ecosystem: Variability and response to El Niño. *Deep Sea Research Part I: Oceanographic Research Papers*, *140*, 52–62. https://doi.org/10.1016/j.dsr.2018.07.012

Nagai, T., Gruber, N., Frenzel, H., Lachkar, Z., McWilliams, J. C., & Plattner, G.-K. (2015). Dominant role of eddies and filaments in the offshore transport of carbon and nutrients in the California Current System. *Journal of Geophysical Research: Oceans*, *120*(8), 5318–5341. https://doi.org/10.1002/2015JC010889

Nencioli, F., d'Ovidio, F., Doglioli, A. M., & Petrenko, A. A. (2011). Surface coastal circulation patterns by in-situ detection of Lagrangian coherent structures. *Geophysical Research Letters*, *38*, L17604. https://doi.org/10.1029/2011GL048815

Ohman, M. D., Barbeau, K., Franks, P. J. S., Goericke, R., Landry, M. R., & Miller, A. J. (2013). Ecological Transitions in a Coastal Upwelling Ecosystem. *Oceanography*, *26*(3), 210–219.

Olivieri, R. A., & Chavez, F. P. (2000). A model of plankton dynamics for the coastal upwelling system of Monterey Bay, California. *Deep Sea Research Part II: Topical Studies in Oceanography*, *47*(5), 1077–1106. https://doi.org/10.1016/S0967-0645(99)00137-X

Omand, M. M., D'Asaro, E. A., Lee, C. M., Perry, M. J., Briggs, N., Cetinić, I., & Mahadevan, A. (2015). Eddy-driven subduction exports particulate organic carbon from the spring bloom. *Science*, *348*(6231), 222–225. https://doi.org/10.1126/science.1260062

Pickett, M. H., & Paduan, J. D. (2003). Ekman transport and pumping in the California Current based on the U.S. Navy's high-resolution atmospheric model (COAMPS). *Journal of Geophysical Research*, *108*, 3327. https://doi.org/10.1029/2003JC001902

Plattner, G.-K., Gruber, N., Frenzel, H., & McWilliams, J. C. (2005). Decoupling marine export production from new production. *Geophysical Research Letters*, *32*, L11612. https://doi.org/10.1029/2005GL022660

Renault, L., Hall, A., & McWilliams, J. C. (2016). Orographic shaping of US West Coast wind profiles during the upwelling season. *Climate Dynamics*, *46*(1–2), 273–289. https://doi.org/10.1007/s00382-015-2583-4

Resplandy, L., Lévy, M., & McGillicuddy, D. J. (2019). Effects of Eddy-Driven Subduction on Ocean Biological Carbon Pump. *Global Biogeochemical Cycles*, *33*(8), 1071–1084. https://doi.org/10.1029/2018GB006125

Resplandy, L., Martin, A. P., Le Moigne, F., Martin, P., Aquilina, A., Mémery, L., et al. (2012). How does dynamical spatial variability impact 234Th-derived estimates of organic export?. *Deep Sea Research Part I: Oceanographic Research Papers*, *68*, 24–45. https://doi.org/10.1016/j.dsr.2012.05.015

Richter, I. (2015). Climate model biases in the eastern tropical oceans: causes, impacts and ways forward. *WIREs Climate Change*, *6*(3), 345–358. https://doi.org/10.1002/wcc.338

Rykaczewski, R. R., & Checkley, D. M. (2008). Influence of ocean winds on the pelagic ecosystem in upwelling regions. *Proceedings of the National Academy of Sciences*, *105*(6), 1965–1970. https://doi.org/10.1073/pnas.0711777105

Sanial, V., Van Beek, P., Lansard, B., Souhaut, M., Kestenare, E., D'Ovidio, F., et al. (2015). Use of Ra isotopes to deduce rapid transfer of sediment-derived inputs off Kerguelen. *Biogeosciences*, *12*(5), 1415–1430. https://doi.org/10.5194/bg-12-1415-2015

Sergi, S., Baudena, A., Cotté, C., Ardyna, M., Blain, S., & d'Ovidio, F. (2020). Interaction of the Antarctic Circumpolar Current with seamounts fuels moderate blooms but vast foraging grounds for multiple marine predators. *Frontiers in Marine Science*, *7*, 416. https://doi.org/10.3389/fmars.2020.00416

Small, R. J., Curchitser, E., Hedstrom, K., Kauffman, B., & Large, W. G. (2015). The Benguela Upwelling System: Quantifying the sensitivity to resolution and coastal wind representation in a global climate model. *Journal of Climate*, *28*(23), 9409–9432. https://doi.org/10.1175/JCLI-D-15-0192.1

Smith, K. L., Ruhl, H. A., Huffard, C. L., Messié, M., & Kahru, M. (2018). Episodic organic carbon fluxes from surface ocean to abyssal depths during long-term monitoring in NE Pacific. *Proceedings of the National Academy of Sciences*, *115*(48), 12235–12240. https://doi.org/10.1073/pnas.1814559115

Stephens, B. M., Wankel, S. D., Beman, J. M., Rabines, A. J., Allen, A. E., & Aluwihare, L. I. (2020). Euphotic zone nitrification in the California Current Ecosystem. *Limnology & Oceanography*, *65*(4), 790–806. https://doi.org/10.1002/lno.11348

Stukel, M. R., Aluwihare, L. I., Barbeau, K. A., Chekalyuk, A. M., Goericke, R., Miller, A. J., et al. (2017). Mesoscale ocean fronts enhance carbon export due to gravitational sinking and subduction. *Proceedings of the National Academy of Sciences*, *114*(6), 1252–1257. https://doi.org/10.1073/pnas.1609435114

Yool, A., Martin, A. P., Fernández, C., & Clark, D. R. (2007). The significance of nitrification for oceanic new production. *Nature*, *447*(7147), 999–1002. https://doi.org/10.1038/nature05885

References From the Supporting Information

Dugdale, R. C., & Goering, J. J. (1967). Uptake of new and regenerated forms of nitrogen in primary productivity. *Limnology & Oceanography*, *12*(2), 196–206. https://doi.org/10.4319/lo.1967.12.2.0196

Harrison, W. G., Platt, T., & Lewis, M. R. (1987). f-Ratio and its relationship to ambient nitrate concentration in coastal waters. *Journal of Plankton Research*, *9*(1), 235–248. https://doi.org/10.1093/plankt/9.1.235

Kishi, M. J., Kashiwai, M., Ware, D. M., Megrey, B. A., Eslinger, D. L., Werner, F. E., et al. (2007). NEMURO–a lower trophic level model for the North Pacific marine ecosystem. *Ecological Modelling*, *202*(1–2), 12–25. https://doi.org/10.1016/j.ecolmodel.2006.08.021

Knauer, G. A., Martin, J. H., & Bruland, K. W. (1979). Fluxes of particulate carbon, nitrogen, and phosphorus in the upper water column of the northeast Pacific. *Deep Sea Research Part A: Oceanographic Research Papers*, *26*(1), 97–108. https://doi.org/10.1016/0198-0149(79)90089-X

Li, Q. P., Franks, P. J. S., Landry, M. R., Goericke, R., & Taylor, A. G. (2010). Modeling phytoplankton growth rates and chlorophyll to carbon ratios in California coastal and pelagic ecosystems. *Journal of Geophysical Research*, *115*(G4), 25–29. https://doi.org/10.1029/2009JG001111

Stukel, M. R., & Barbeau, K. A. (2020). Investigating the nutrient landscape in a coastal upwelling region and Its relationship to the biological carbon pump. *Geophysical Research Letters*, *47*(6), e2020GL087351. https://doi.org/10.1029/2020GL087351

Stukel, M. R., Benitez-Nelson, C. R., Décima, M., Taylor, A. G., Buchwald, C., & Landry, M. R. (2016). The biological pump in the Costa Rica Dome: an open-ocean upwelling system with high new production and low export. *Journal of Plankton Research*, *38*(2), 348–365. https://doi.org/10.1093/plankt/fbv097

Stukel, M. R., Kahru, M., Benitez-Nelson, C. R., Décima, M., Goericke, R., Landry, M. R., & Ohman, M. D. (2015). Using Lagrangian-based process studies to test satellite algorithms of vertical carbon flux in the eastern North Pacific Ocean. *Journal of Geophysical Research: Oceans*, *120*(11), 7208–7222. https://doi.org/10.1002/2015JC011264

Stukel, M. R., Kelly, T. B., Aluwihare, L. I., Barbeau, K. A., Goericke, R., Krause, J. W., et al. (2019). The Carbon:234Thorium ratios of sinking particles in the California current ecosystem 1: relationships with plankton ecosystem dynamics. *Marine Chemistry*, *212*, 1–15. https://doi.org/10.1016/j.marchem.2019.01.003

Stukel, M. R., Landry, M. R., Benitez-Nelson, C. R., & Goericke, R. (2011). Trophic cycling and carbon export relationships in the California Current Ecosystem. *Limnology & Oceanography*, *56*(5), 1866–1878. https://doi.org/10.4319/lo.2011.56.5.1866